Electrochimica Acta 55 (2009) 498–503

Contents lists available at ScienceDirect

Electrochimica Acta

journal homepage: www.elsevier.com/locate/electacta

Effective corrosion protection of AA6061 aluminum alloy by sputtered Al–Ce coatings

M.A. Domínguez-Crespo[a,*], A.M. Torres-Huerta[a], S.E. Rodil[b], E. Ramírez-Meneses[a], G.G. Suárez-Velázquez[c], M.A. Hernández-Pérez[d]

[a] Instituto Politécnico Nacional, GIPMAT CICATA-Altamira, km 14.5, Carretera Tampico-Puerto Industrial Altamira, C.P. 89600 Altamira, Tamps, Mexico
[b] Instituto de Investigación en Materiales, Universidad Nacional Autónoma de México, Circuito Exterior s/n, Ciudad Universitaria, Del. Coyoacán, C.P. 04510 México, D.F., Mexico
[c] Alumna del PTA del CICATA-Altamira IPN, km 14.5, Carretera Tampico-Puerto Industrial Altamira, C.P. 89600 Altamira, Tamps, Mexico
[d] Instituto Politécnico Nacional, ESIQIE, C.P. 07738 México, D.F., Mexico

ARTICLE INFO

Article history:
Received 26 May 2009
Received in revised form 3 September 2009
Accepted 3 September 2009
Available online 9 September 2009

Keywords:
AA6061
Magnetron sputtering
Coatings
Corrosion properties
Al–Ce films

ABSTRACT

Al–Ce coatings were deposited on silicon and AA6061 aluminum alloy substrates by DC magnetron sputtering using aluminum in combination with pure cerium targets. The materials were characterized by X-ray diffraction (XRD), atomic force microscopy (AFM), scanning electron microscopy (SEM), high resolution transmission electron microscopy (HRTEM) and electrochemical impedance spectroscopy (EIS) in order to consider their application as high corrosion resistance coatings. The corrosion behavior of the films was studied using a NaCl aqueous solution (3.5 wt%). As for the characterization results, an apparent amorphous phase of aluminum oxide with small cerium compounds embedded in the matrix was detected by the X-ray diffraction patterns and HRTEM on the deposited films at 200 W and 4 Pa. At these conditions, AFM and SEM images evidenced crack-free coatings with low-roughness nanometric structures and columnar growth. EIS and Tafel results converged to indicate an inhibition of the corrosion reactions. The film displayed good stability in the aggressive medium and after 1 day of exposure underwent very little degradation. The variations in the impedance and Tafel characteristics were found to occur as a function of cerium content, which provokes important changes in the film protective properties.

1. Introduction

Aluminum is one of the main components of common alloys used in different applications. Aluminum, when alloyed with small amounts of other materials, is an essential and valuable metal because of its high specific strength and low density. However, untreated Al–Mg–Cu based alloys like AA2024, AA6061 and AA7075 are susceptible to corrosion [1]. The main corrosion process that is developed on the surface of aluminum alloys in a NaCl solution is the localized alkaline corrosion in the aluminum matrix surrounding Al(Mn, Fe, Cr) cathodic intermetallics [2]. Thus, in order to protect the alloy, it is necessary to design a process to block the cathodic reaction over the cathodic precipitates in order to allow the formation of the aluminum oxide film onto the metallic matrix. The application of protective coatings such as chromate conversion coatings are commonly used in aluminum alloys. This method is relatively simple; however, the environmental and health risks associated with the use of chromate ions are restricted now. It is, therefore, necessary to investigate other, nontoxic or less toxic coating processes with equal or even better corrosion protection. Since the mid-1980s, Ce conversion layers have been studied as a promising alternative to protect aluminum alloys. Many works have been published about different methods and conditions to obtain Ce conversion layers on several Al substrates that are of interest to the aircraft industry and their microstructure and corrosion behavior have been investigated [3–7]. However, some drawbacks of cerium conversion layers obtained from conventional methods are: (i) the precipitation of an insoluble protective Ce oxide/hydroxide layer that produces coatings with uneven characteristics; (ii) the presence of cracks that can cross the whole cross-section of the layer. These cracks represent preferential pathways for the penetration of aggressive species, although in this case the layer seems to exhibit self-healing ability, which helps its long-term protection properties. On the other hand, the flexibility and control of process conditions have established magnetron sputtering as a widely used deposition technique. In this process, the particles arriving at the substrate have enough energy to diffuse and migrate on the surface forming a dense crystalline film [8,9].

* Corresponding author. Tel.: +52 55 57 29 6000x87512.
E-mail addresses: mdominguezc@ipn.mx, adcrespo2000@yahoo.com.mx (M.A. Domínguez-Crespo).

0013-4686/$ – see front matter © 2009 Elsevier Ltd. All rights reserved.
doi:10.1016/j.electacta.2009.09.002

According to the aforementioned, the development of new environmentally friendly and protective coatings to enhance the anticorrosive properties of materials is of great research interest. As far as we know, sputtered Al–Ce coatings to enhance the properties against corrosion of aluminum alloys have not been reported yet. The data reported in this paper are a portion of the research project (sponsored by Science and Technology National Council of Mexico, CONACYT) for studying the anticorrosive properties of sputtered Al-rare earth coatings and propose new alternatives to improve the corrosion resistance of aluminum alloys. Specifically, the work presented here is focused on the electrochemical corrosion of Al–Ce thin films deposited on AA6061 aluminum alloy by magnetron sputtering.

2. Experimental

Samples of AA6061 aluminum in the form of discs were ground up to 600-grade SiC paper, cleaned with water and ethanol in an ultrasonic bath for 20 min before processing. The dimensions of the selected specimens for coating during the structural characterization and electrochemical corrosion test were: 25 mm in diameter and 2 mm in thickness. Aluminum-based coatings were deposited by means of a commercial pulsed DC magnetron sputtering apparatus, from a multicomponent target consisting of Al (99.95% purity, 100 mm in diameter and 3 mm in thickness) and eight Ce pieces (99.5% purity, 15 mm × 5 mm × 1 mm) attached to the aluminum target race track. The system was initially pumped to a vacuum pressure of 1.33×10^{-4} Pa. The deposition was done using Ar (99.99% purity) atmosphere at flow rates between 10 and 14 sccm. To study the effect of pressure and power on film composition and their influence on corrosion behavior, two sets of experiments were carried out. In the first set, pressure was increased from 6.67×10^{-1} to 4 Pa at 200 W and in the second set; power was varied from 40 to 280 W at a constant pressure of 4 Pa. The other deposition parameters were kept constant: the substrate temperature was not controlled, but previous studies showed that the maximum reached value was 80 °C with a deposition time of 300 s, the substrate was ground without bias and the substrate-to-target distance (ds–t) was fixed at 5 cm [10]. The coatings were also simultaneously deposited onto silicon (1 1 1) and both substrates were chosen for their suitability for the particular analysis techniques. The samples deposited on the substrates were used for structural and morphological characterization by XRD, AFM, SEM and HRTEM; while thickness was determined by profilometry and SEM. The XRD measurements of the films were performed by a Brucker D8 series diffractometer with Cu Kα (λ = 0.154 nm) radiation while atomic force microscopy studies were carried out in a Nanosurf easyscan 2.0 microscope. The morphological and chemical aspects of the coatings were studied by scanning electron microscopy (SEM/EDS) using a JEOL JSM-35C. HRTEM studies were carried out on a JEOL 2010 FasTem field emission transmission electron microscope with a resolution of 2.1 Å. The corrosion behavior of the coated and uncoated aluminum alloy was determined by Tafel and electrochemical impedance spectroscopy measurements. A potentiostat/galvanostat (Gamry 600 series) using a graphite bar as the counter electrode and a saturated calomel electrode (SCE) as reference electrode, was employed to perform corrosion experiments. An electrochemical cell consisting of an acrylic rectangular box (60 mm × 80 mm × 100 mm) was used and the exposed area of the sample was 1.23 cm^2. The specimens were introduced by moderate pressure against an o-ring, avoiding localized damage to the thin films. The Tafel polarization curves were measured from the cathodic to anodic area. The scans were started at −250 mV *vs* SCE with a sweep rate of 1 mV s^{-1}. The EIS measurements were carried out in the frequency region from 100,000 to 0.01 Hz (ten frequency points per decade) with an amplitude of 10 mV rms.

3. Results and discussion

3.1. Surface morphology and microstructure of the coatings

Fig. 1a and b shows the dependence of the deposition rate (film thickness/deposition time) on the applied pressure and power in the sputtering chamber for the Al–Ce films grown on the Si substrate. It can be seen that the deposition rate was increased as pressure was also increased at constant power (Fig. 1a). A maximum thickness value was reached at 4 Pa (∼1200 nm). In order to optimize the deposition process, the next set of experiments was carried out by varying power at 4 Pa. The deposition rate gradually increased as power was increased to 200 W, where a slight decrease is observed from 4.04 to 3.90 nm s^{-1} (Fig. 1b). The deposition rate drop could be due to resputtering of the as-deposited film, i.e. kicking off the adatoms or growing surface by the incoming ions [11]. Due to the fact that protection in a chloride-containing environment depends on the quantity of cerium to form oxide/hydroxide compounds, in this work, only the results for the maximum content of cerium (∼30% forming the film, at 200 W and 4 Pa) on the substrate surface are shown.

An amorphous phase and crystalline reflections of oxide compounds can be seen from the XRD analysis of the Al–Ce coatings on silicon substrates (Fig. 2). Although the deposition process was carried out under inert atmosphere, oxide compounds were obtained as a result of the high reactivity of the aluminum and cerium under room condition thus, it is very likely that the oxides were formed once the samples were exposed to the atmosphere. The peak around 55.7° belongs to the Si (1 1 1) substrate, in the oriented reflection (3 1 1) underneath the film. The as-deposited films showed weak signals of the planes (2 0 2), (1 1 6) positioned at 41.03° and 54.5°, which belong to $CeAlO_3$. Additionally, the presence of aluminum oxide (Al_2O_3) and cerium oxide (Ce_2O_3) was

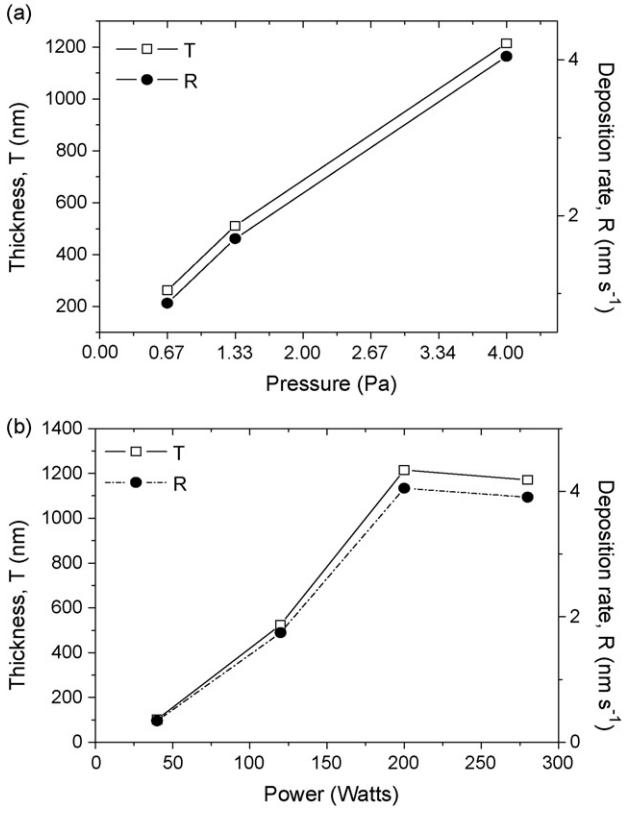

Fig. 1. Deposition rate and thickness of the film as functions of: (a) total pressure and (b) power.

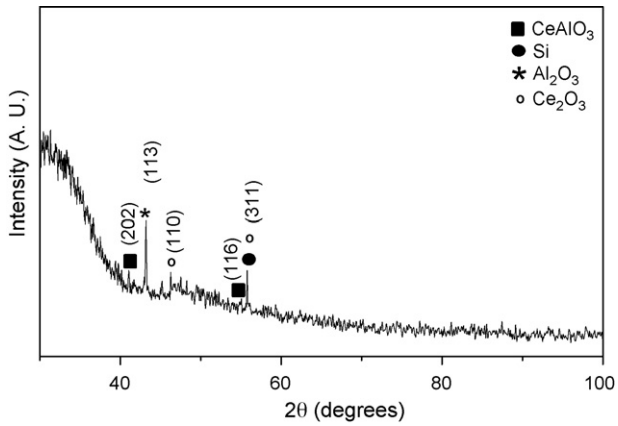

Fig. 2. XRD pattern of Al–Ce coatings on silicon at 4 Pa and 200 W.

observed at 43.19° and 46.2°, respectively. The observed reflections are possibly due to the smallest surface energy storage in the stressed state. The morphology and size distribution of the particles on silicon (created at 4 Pa, 200 W and a gas flow rate of 10 sccm) obtained by image data analysis through contact mode AFM and the Nanosurf software are shown in Fig. 3a and b. The surface of these films consisted of uniform, compact with small pores and smoother domes uniformly covering the substrate. Fig. 4a–c shows a representative EDS analysis and images corresponding to the sputtered films on AA6061 aluminum alloy. The EDS investigation identified an important cerium quantity (31.41 wt%) which was homogeneously distributed in the whole metallic surface. In addition, some aluminum and oxygen quantity was observed in the analysis. From these results, the Ce content increased as increases the film thickness. The morphology of these films matched with the observed morphology on silicon substrates, suggesting that the substrate do not influence the Al–Ce film growth (Fig. 4b). Fig. 4c shows the cross-section of Al–Ce coatings obtained by SEM measurements and whose thickness is about 1200 nm. The HRTEM image and its corresponding selected area diffraction pattern (SADP) of Al–Ce coatings on metallic substrates are shown in Fig. 5. The micrograph also shows nanometric structure, low-roughness and crack-free coatings. From XRD and HRTEM results, two phases can be distinguished: an apparent amorphous phase corresponding to aluminum oxide and small cerium compound crystals embedded in the amorphous matrix. The results indicate that the unstructured phase formed in the samples prepared via the sputtering technique depends on the following features: (a) the molar ratio of aluminum to cerium and (b) operating conditions (power and pressure).

Table 1
Corrosion potential and corrosion current densities of selected coated and uncoated samples.

Parameter	Sample	
	Bare aluminum	Coated sample
E_{corr} (V)	−0.807	−1.224
i_{corr} (A cm^{-2})	1.7×10^{-7}	2.6×10^{-8}

3.2. Electrochemical characterization of the coatings

In order to assess the degree of the protection afforded by the sputtered coatings, selected coated and uncoated specimens were subjected to Tafel analysis. These plots were obtained from the Al–Ce films at 4 Pa, 200 W in a 3.5 wt% NaCl solution (Fig. 6). The Tafel extrapolations show that at these experimental conditions the Al–Ce coatings cause a negative shift of around 400 mV in the corrosion potential in comparison with the bare aluminum, which can be characteristic of the cathodic inhibition [2] and is related to the interaction between cerium and aluminum oxides forming the film. It is known that for aluminum alloys, corrosion can be considered as a combination of at least two electrochemical reactions involving anodic areas where metal dissolution occurs; $Al \rightarrow Al^{3+} + 3e^{-}$ and cathodic areas where reactions such as the reduction of oxygen takes place, $O_2 + 2H_2O + 4e^{-} \rightarrow 4OH^{-}$ [12,13]. Then, from these results both necessary reactions of corrosion were suppressed by the Al–Ce coatings thereby reducing the driving force of the corrosion process. The plots also shifted towards lower current densities which resulted in the decrease of the overall corrosion. In Table 1, the corrosion current densities and free corrosion potential obtained for coated and uncoated samples are summarized. It was noticed that the overall current density calculated from the Tafel extrapolation curves decreased on the deposited films in comparison with the substrate and it is also better than the obtained results for the cerium-based conversion layers [5].

The impedance spectra can be used to evaluate the corrosion protection afforded by sputtered coatings and to provide adequate modeling of the physicochemical processes on the coated substrate during corrosion tests [14,15]. The EIS measurements of the Al–Ce oxide coatings were performed after 24 h of continuous immersion in NaCl solution and the representative plots are presented in Fig. 7. As it can be seen from this figure, a depressed semicircle shape concerning the coatings and a diffusion tail (Warburg impedance, *W*) in the low frequency region are observed. The deviation from the ideal

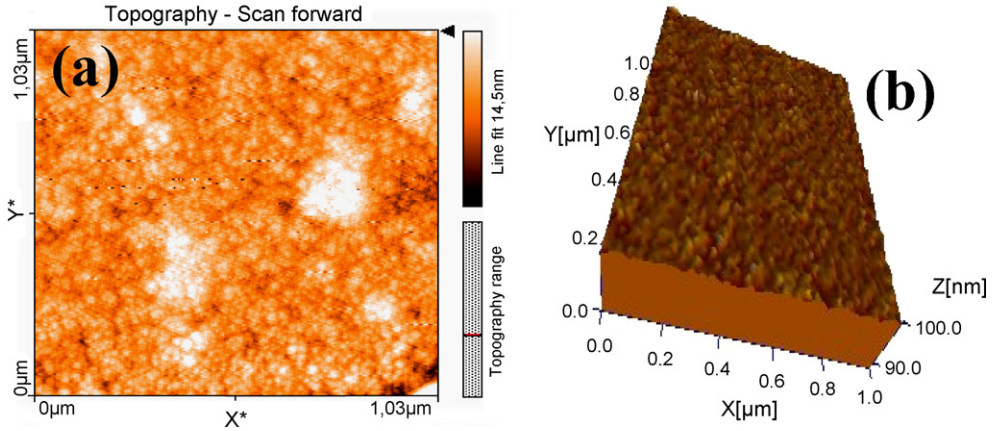

Fig. 3. AFM images (1 μm × 1 μm) of the samples as-grown on silicon at 200 W and 4 Pa: (a) topography and (b) 3D mapping showing the growth morphologies of ~230 nm films.

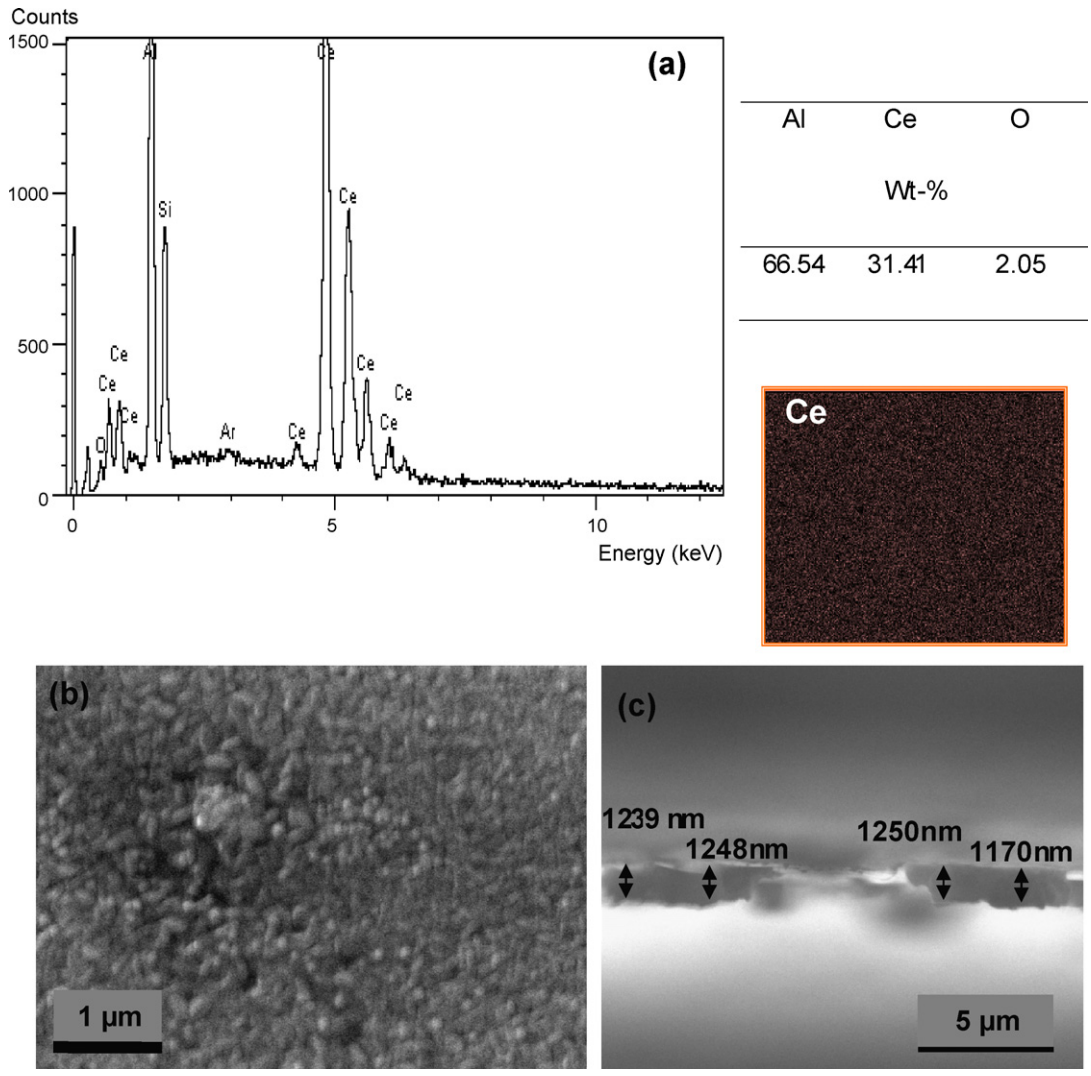

Fig. 4. Scanning electron micrographs of Al–Ce coatings on AA6061 aluminum alloy at 200 W and 4 Pa for 300 s: (a) EDS and mapping analysis, (b) surface view and (c) cross-section view.

semicircle is related to the surface inhomogeneities (domes) of the coatings. The solid line in this figure represents the fitted EIS spectra based on the equivalent circuit which are shown in the inset figure. The EIS data were fitted based on the electrical equivalent diagrams suggested in the literature to model metal + coating-solution interface (pits) for Al based materials [16,17] and the calculated data are also given in Table 2. The dependence of the complex impedance of the coated aluminum on the applied frequency allows separation of the responses of the different components of the system such as capacitance and resistance of the protective layers and oxide films. In the circuit R_s, R_{film} and R_{ct} are the electrolyte resistance, film resistance and charge transfer resistance which is commonly cor-

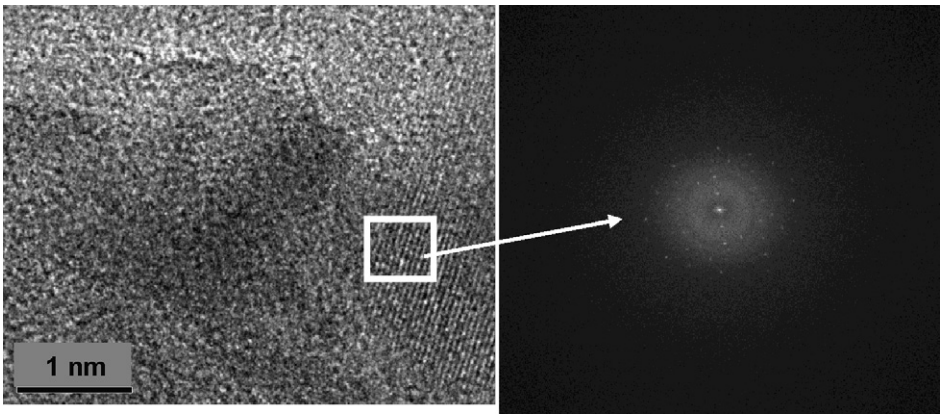

Fig. 5. HRTEM image and selected area diffraction pattern (SADP) of Al–Ce coatings on metallic substrates at 200 W and 4 Pa for 300 s.

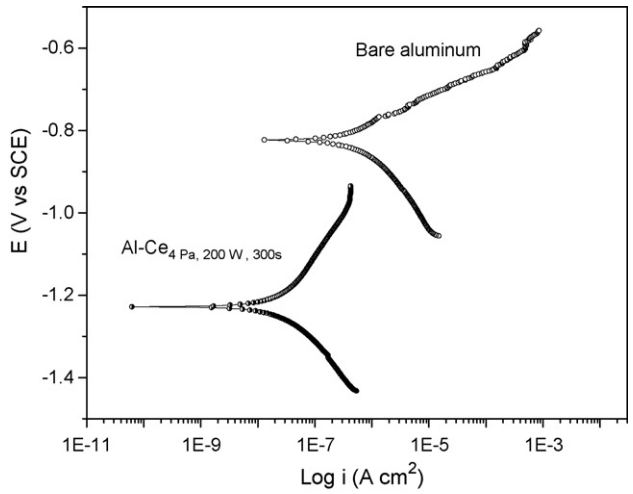

Fig. 6. Tafel curves for the AA6061 aluminum alloy without (frame circle) and with (solid circle) coating after 24 h of testing.

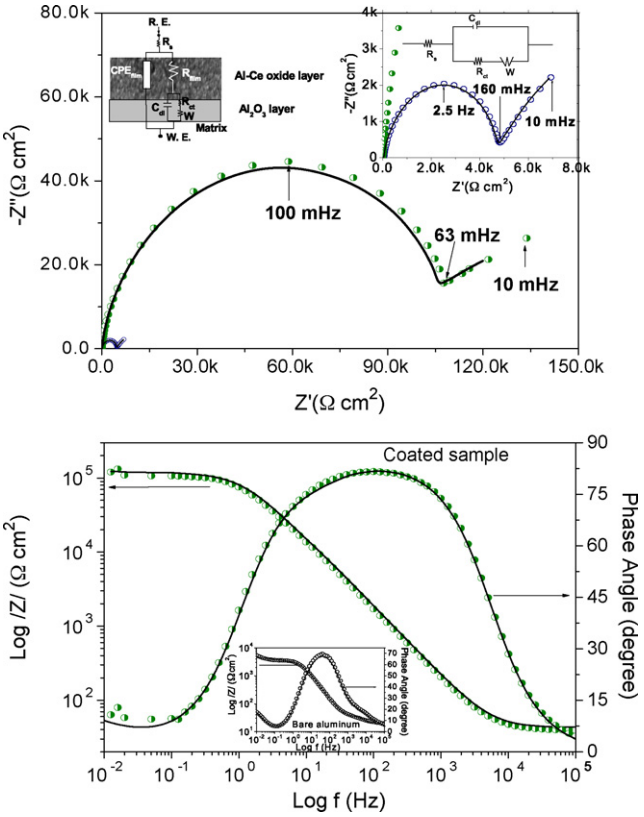

Fig. 7. Nyquist and Bode spectra with their corresponding equivalent circuit used during the simulation of the bare substrate (frame circle) and Al–Ce coatings (solid circle) and fitted parameters (solid line).

Table 2
Fitted parameters determined from Nyquist plots.

Parameter	Sample	
	Bare aluminum	Coated sample
R_s ($\Omega\,cm^2$)	18.23	17.39
R_{film} ($k\Omega\,cm^2$)	–	115.91
Y_{ofilm} ($\Omega^{-1}\,s^n$)	–	3.29
n_{film}	–	0.93
C_{dl} ($\mu F\,cm^{-2}$)	1.84	5.69
R_{ct} ($k\Omega\,cm^2$)	4.956	7.65
W ($\Omega^{-1}\,s^{0.5}$)	218.5	294.5
χ^2	0.547E−3	0.661E−3

related to localized corrosion, respectively; whereas C_{film}, and C_{dl} represent the capacitance of the film and double layer during corrosion process, respectively. W is the Warburg element that accounts for the diffusion controlled process. In addition, to justify the non-homogeneity of the electrochemical systems, pure capacitors were substituted by a constant phase element (CPE). The EIS data for the bare aluminum show very low impedance at all frequency ranges, whereas the Al–Ce oxide films presented a high frequency capacitive loop that is correlated with the high cerium content in the film (Table 2). Corrosion resistant surfaces for AA6061 aluminum alloy were obtained by the magnetron sputtered Al–Ce coatings. The polarization resistance R_p (the combination of the resistances involved in the corrosion process) was about 5460 $\Omega\,cm^2$ for the bare aluminum, while it was close to 135 $k\Omega\,cm^2$ for samples coated with the Al–Ce coatings at the aforementioned deposition parameters. Thus, the charge transfer resistance (R_{ct}) was increased when the Al–Ce coatings were added to the substrate. The lowest double layer capacitance (C_{dl}) values also indicate the highest protection presented in the aggressive medium. No corrosion was visually found in the coated substrates after 24 h of continuous immersion in the electrolyte. This fact indicates that the major event was water/ion penetration into the Al–Ce oxide film, which resulted in the saturation of the coating with the electrolyte. On the basis of previous characterization works for different cerium coatings on aluminum alloys [18,19], two different regions from the outside Al–Ce films to substrate are proposed: a porous surface composed of uniform, compact smother domes combined with extensively dense Al–Ce interfacial layer on the alloy substrate and the inner alumina layer on the alloy substrate as it is illustrated in the inset in Fig. 7. Hence, the electrochemical results (after application of protective coating) show that the protective properties of the Al–Ce coatings increased as increasing cerium content due to the inhibition of both anodic and cathodic reactions. Afterward, the Al–Ce oxides in the outer layer of the passive films function as a barrier layer.

The obtained values for the bare samples are considerably different from those concerning the coated samples because the protection of the substrate is deeply modified by the coating process. The corrosion performance of the Al–Ce coatings can be correlated with a denser coating that resulted from the formation of fine $CeAlO_3$ and Ce_2O_3 particles. Then, the coatings could act as a good protective barrier to prevent the corrosive environment from reaching and reacting with the substrate metal. The structure of the deposited $CeAlO_3$ coatings does not match any of the previously reported structures of cerium compounds with anti-corrosion properties and it depends on cerium loading [18]. The results are comparable with the technological process of Ce sealing of anodized aluminum alloys [19], ceria sol–gel coatings [20] and those showed by cerium-based conversion layers on aluminum alloys [6]. However, since the protection level strongly depends on the specimen preparation prior to deposition [21], it might be still possible to improve the performance against corrosion of the sputtered Al–Ce oxide films on aluminum alloys [22], by analyzing the effect of the substrate surface preparation prior to deposition and established the connection between the microstructure of the Al–Ce thin films and deposition parameters, which is a work that is currently in progress.

4. Conclusions

Al–Ce coatings deposited by magnetron sputtering on AA6061 aluminum alloy were characterized by different techniques in order to study their possible applications as protective barriers in aggressive media. It was found that at 200 W and 4 Pa, the Al–Ce coatings were mainly composed of Al_2O_3, $CeAlO_3$ and Ce_2O_3 particles with a dense amorphous structure with small crystalline cerium com-

pounds embedded in the matrix. The electrochemical performance indicated that the Al–Ce coatings function as protective barriers inhibiting the corrosion reactions, which is promising to delay pitting corrosion of the aluminum alloys. Finally, the deposition parameters have a strong influence in the barrier properties of the film, which is related with Ce content and thickness.

Acknowledgements

This study has been financially supported by CONACYT (project number 61354), IPN (projects number SIP-2009-0561, 2009-0499) and SNI. The authors would like to thank Dr. David Turcio-Ortega, Mr. Javier Zapata Torres and H. Zarco for technical support.

References

[1] H. Schâfer, H.R. Stock, Corr. Sci. 47 (2005) 953.
[2] M. Bethencourt, F.J. Botana, M.J. Cano, M. Marcos, Appl. Surf. Sci. 238 (2004) 278.
[3] L.E.M. Palomino, J.F. de Castro, I.V. Aoki, H.G. de Melo, J. Brazil Chem. Soc. 14 (2003) 651.
[4] P. Campestrini, H. Terryn, A. Hovestad, J.H.W. Wit, Surf. Coat. Technol. 176 (2004) 365.
[5] M. Dabalà, L. Armelao, A. Buchberger, I. Calliari, Appl. Surf. Sci. 172 (2001) 312.
[6] A.E. Hughes, R.J. Taylor, B.R.W. Hinton, L. Wilson, Surf. Interf. Anal. 23 (2004) 540.
[7] F. Mansfeld, Y. Wang, Appl. Surf. Sci. 198 (1995) 51.
[8] S.D. Ekpe, L.W. Bezuidenhout, S.K. Dew, Thin Solid Films 474 (2005) 330.
[9] S.D. Ekpe, S.K. Dew, J. Vac. Sci. Technol. 20 (2002) 1877.
[10] J.J. Olaya, S.E. Rodil, S. Muhl, E. Sánchez, Thin Solid Films 474 (2005) 119.
[11] X. Pang, L. Shi, P. Wang, G. Zhang, W. Liu, Surf. Coat. Technol. 203 (2009) 1537.
[12] X. Yu, C. Cao, Z. Yao, D. Zhou, Z. Yin, Corr. Sci. 43 (2001) 1283.
[13] X. Yu, D. Zhou, Z. Yin, Chin. J. Nonferrous Met. 9 (1999) 73.
[14] M.L. Zheludkevich, R. Serra, M.F. Montemor, K.A. Yasakau, I.M. Miranda Salvado, M.G.S. Ferreira, Electrochim. Acta 51 (2005) 208.
[15] B.R. Hinderliter, S.G. Croll, D.E. Tallman, Q. Su, G.P. Bierwagen, Electrochim. Acta 51 (2006) 4505.
[16] F. Mansfeld, S. Lin, S. Kim, H. Shih, J. Electrochem. Soc. 137 (1990) 78.
[17] D. Zhu, W.J. Van Ooij, Corros. Sci. 45 (2003) 2177.
[18] I. Avramova, P. Stefanov, D. Nicolova, D. Stoychev, Ts. Marinova, Compos. Sci. Technol. 65 (2005) 1663.
[19] Y. Xingwen, C. Chunan, Thin Solid Films 423 (2003) 252.
[20] A.S. Hamdy, D.P. Butt, A.A. Ismail, Electrochim. Acta 52 (2007) 3310.
[21] A.S. Hamdy, A.M. Beccaria, J. Appl. Electrochem. 35 (2005) 473.
[22] F.B. Rivera, Y.B. Jhonson, J.M. O'Keefe, G.W. Fahrenholtz, Surf. Coat. Technol. 176 (2004) 349.